[CANCER RESEARCH 62, 6278–6288, November 1, 2002]

Single Cell Behavior in Metastatic Primary Mammary Tumors Correlated with Gene Expression Patterns Revealed by Molecular Profiling[1,2]

Weigang Wang,[3] Jeffrey B. Wyckoff,[3] Victoria Centonze Frohlich, Yuri Oleynikov, Stefan Hüttelmaier, Jiri Zavadil, Lukas Cermak, Erwin P. Bottinger, Robert H. Singer, John G. White, Jeffrey E. Segall, and John S. Condeelis[4]

Departments of Anatomy and Structural Biology [W. W., J. B. W., Y. O., S. H., R. H. S., J. E. S., J. S. C.] and Medicine [J. Z., L. C., E. P. B.], Albert Einstein College of Medicine, Bronx, New York 10461; Department of Cellular and Structural Biology, University of Texas Health Science Center at San Antonio, San Antonio, Texas 78229 [V. C. F.]; and Department of Anatomy, University of Wisconsin-Madison, 1525 INDEN DR, Madison, Wisconsin 53706 [J. G. W.]

ABSTRACT

We have developed animal models of breast cancer that allow the direct examination of the behavior of individual green fluorescent protein-expressing carcinoma cells in live nonmetastatic and metastatic primary tumors *in situ*. We have combined this model with multiphoton microscopy to image differences in cell behavior within the primary tumor. Differences in cell behavior between nonmetastatic and metastatic cells in culture and within live primary tumors were correlated with results from cDNA microarray analyses to identify potentially important genetic determinants for breast cancer invasion and metastasis. Using multiphoton microscopy, we found five major differences in carcinoma cell behavior between the nonmetastatic and metastatic primary breast tumors involving extracellular matrix, cell motility, and chemotaxis. Behavioral differences were correlated with seven categories of molecules that were differentially expressed and related to these behaviors. We have found that extracellular matrix composition, actin nucleation factors, molecules involved in mechanical stability and survival, and cell polarity and chemotaxis showed large and consistent differences in gene expression. We conclude that aligning cell behavior *in vivo* with patterns of gene expression can lead to new insights into the microenvironment of carcinoma cells in the primary tumor and the molecular mechanisms behind cell behavior.

INTRODUCTION

Metastasis is believed to involve the escape of carcinoma cells from the primary tumor via lymphatics and blood vessels, transport to and arrest in a target organ, and growth of metastases in the target organ (1). Each of these steps is a multicomponent process, with families of molecules playing critical roles at different steps. Much work has gone into characterizing metastasis at the late steps from extravasation onward using experimental metastasis, in which carcinoma cells are injected into the circulation of host animals (2, 3). This has led to insights into the adhesion, proteolysis, and proliferation mechanisms that cause metastatic tumors. However, the primary tumor has remained a black box at the single-cell level.

The development of high-density molecular arrays has led to the identification of new genes and proteins that contribute to specific steps in metastasis within the primary tumor (4, 5). Such approaches are crucial in the analysis of cancer as a genetic disease and in the identification of patterns of gene expression that might be used in diagnosis and therapy. However, array-based analyses of whole tumors still treat the tumor as a black box. The discovery of specific genes that correlate with metastatic potential cannot be related to mechanism unless the metastatic step at the cellular level in which the gene is involved is identified. Ideally, high-resolution methods for the analysis of metastasis at the cellular level, such as imaging of cells within tumors, when combined with array-based approaches, could be used to accurately evaluate the roles of specific gene products in the individual steps of metastasis. To this end, the development of laser capture microdissection has been an important advance (6). However, the identification of cells within the tumor relies on morphology within fixed tissue, making the identity of the collected cells and their behavior within the tumor before fixation uncertain. Therefore, we have developed high-resolution methods for imaging cells within tumors.

We have used a model of breast cancer that allows the direct examination of the behavior of individual carcinoma cells in live nonmetastatic and metastatic primary tumors *in situ* (7, 8). The nonmetastatic and metastatic tumor cell lines used to create the tumors by s.c. injection are the MTC and MTLn3 cell lines, respectively. These cell lines represent a well-characterized cell pair that were derived from the same original tumor and retain their relative metastatic phenotypes after prolonged culture (9, 10). These cell lines were engineered to constitutively express GFP[5] (7). Upon s.c. injection of these cells into the mammary fat pad of female Fischer 344 rats, primary tumors form that contain fluorescent carcinoma cells. Furthermore, GFP expression does not affect the growth, histology, and metastasis of the primary tumor (7, 11, 12). With this model, the behavioral phenotypes of cells within metastatic and nonmetastatic tumors have been described and differentiated (7, 9). In principle, this model can be extended to any type of tumor cell that grows as a primary tumor s.c. It was the first model that allowed direct observations of invasive and metastatic cell behaviors in intact orthotopically grown primary tumors while in a live animal without the need for a viewing window and has made the primary tumor available for direct analysis at the single-cell level.

Recently, multiphoton microscopy, a powerful tool that combines laser scanning confocal microscopy with multiphoton excitation of fluorescence to create high-resolution, three-dimensional images of microscopic samples, has been introduced. This technique is particularly valuable in the study of cell behavior *in vivo* because it can be used to probe delicate living tissues at great depths and cellular resolution without damaging the sample (13, 14). In this study, we have combined our GFP-carcinoma cell models with multiphoton microscopy to image differences in cell behavior within the primary tumor. In addition, we have correlated differences in cell behavior with array-based approaches to directly associate cell behavior with gene expression and evaluate the roles of specific gene products in the individual steps of metastasis. This is the first time that these tech-

Received 5/16/02; accepted 9/11/02.

The costs of publication of this article were defrayed in part by the payment of page charges. This article must therefore be hereby marked *advertisement* in accordance with 18 U.S.C. Section 1734 solely to indicate this fact.

[1] Supported by United States Department of Defense Grant BC980718, NIH Grant CA 89829, grants from the National Institute of General Medical Sciences, and United States Department of Energy Grant DE-FG02-00ER63056. Real-time PCR was supported by Grant 1U24DK58768-01A1.

[2] Supplementary data for this article are available at Cancer Research Online (http://cancerres.aacrjournals.org).

[3] These authors contributed equally to this work.

[4] To whom requests for reprints should be addressed, at Department of Anatomy and Structural Biology, Albert Einstein College of Medicine, 1300 Morris Park Avenue, Bronx, NY 10461. E-mail: condeeli@aecom.yu.edu.

[5] The abbreviations used are: GFP, green fluorescent protein; ECM, extracellular matrix; QRT-PCR, quantitative real-time PCR; AECOM, Albert Einstein College of Medicine; NSI, net signal intensity; EGF, epidermal growth factor; EGFR, EGF receptor; FGF, fibroblast growth factor; IGF, insulin-like growth factor; PAK, p21/Cdc42/Rac1-activated kinase.

niques have been combined in this way. It is a novel approach to gene discovery in invasion and has made the primary tumor available for direct analysis at the single-cell level.

MATERIALS AND METHODS

Cell Culture and Tumor Growth. Rat mammary adenocarcinoma MTLn3 and MTC cell lines transfected with GFP were used in this study. Their metastatic potentials (high metastatic potential for MTLn3 cell line; low metastatic potential for the MTC cell line) have been described previously (9–11). Cells were maintained in α-modified MEM (Life Technologies, Inc.) containing 5% fetal bovine serum and antibiotics (penicillin and streptomycin). MTLn3 and MTC cells were injected into female Fischer 344 rats (1×10^6 cells/rat) as described previously, and tumors were allowed to grow for 2.5 weeks.

Anesthesia and Surgery of Tumor-bearing Animals. Tumor imaging was performed as described below. Briefly, 1×10^6 cells were injected under the second nipple anterior from the tail of a Fischer 344 rat and allowed to grow for 2.5 weeks. After 2.5 weeks, rats were placed under anesthesia with 5% isoflurane and maintained for the course of the imaging session at 2.5% to 0.5% isoflurane to control constant breathing. Minimal surgery was performed to expose the tumor by removing a small skin flap with as little damage to surrounding blood vessels as possible. The animal was placed on an inverted microscope and imaged at 960 nm for GFP fluorescence. For visualizing vasculature, 200 μl of rhodamine-dextran (2 M Dalton; Sigma Chemical Co.) at 20 mg/ml in Dulbecco's PBS were injected into the tail vein of the rat after anesthesia but before surgery.

Multiphoton Microscopy. A 10 W Millennium Xs laser (Spectra Physics) was used to run a Radiance 2000 multiphoton system (Bio-Rad, Hercules, CA) that gives an output of 850 mW at 960 nm. For GFP fluorescence, 960 nm is the optimal imaging wavelength. Time-lapsed images of GFP-labeled MTLn3- and MTC-generated tumors were taken at 60-s intervals for 30 min. The images were collected using Bio-Rad's Lasersharp 2000 software at 50 lines/s and a Kalman of 4. Images were processed using NIH Image 1.61/ppc and Adobe Photoshop. Pixel intensity of fluorescence and second harmonic-generated photons was quantified by subtracting the background from the total pixel intensity of the region of interest.

Measurement of Cell Behavior. Cell motility and adhesion were visualized by time-lapse multiphoton microscopy by taking an image at 1-min intervals for at least 30 min. Each Kalman averaged image required 10 s for collection giving good spatial resolution for cells moving 10 μm/min and less. Motion analysis was carried out using 2D DIAS image analysis software (15).

Microarray Procedures. Total RNA was isolated from MTLn3 and MTC cell or tumor using Trizol reagent (Life Technologies, Inc.). The RNA quality was verified by electrophoresis on a formaldehyde-1.2% agarose gel.

Microarray analysis was performed by using cDNA microarrays made at AECOM (16). About 9,700 mouse genes (Incyte Genomics) were precisely spotted onto a single glass slide. Detailed descriptions of microarray hardware and procedures are available online.[6] The use of these mouse arrays with rat RNA has been validated and shown to have more than 90% correlation between these two species.[7] This result was further validated by real-time PCR as described in this study (Fig. 7).

Microarray analysis was performed in three independent repeats. For each hybridization, cDNA targets were prepared from the RNA samples obtained from MTLn3 (Cy5-labeled) and the MTC (Cy3-labeled) cells or tumor. Labeling and hybridization were performed as follows: first-strand cDNA probes were generated by incorporation of either Cy3-dUTP or Cy5-dUTP (Amersham Pharmacia) during reverse transcription of 100 μg of total RNA. The resulting cDNA probes were purified and concentrated, denatured at 94°C, and hybridized to an arrayed slide overnight at 50°C. Slides were then washed in 1× SSC/0.1% SDS for 10 min and then washed in 0.2× SSC/0.1% SDS for 20 min. Slides were then rinsed and dried, and then they were ready for scanning. Data from the hybridization reactions were collected using a two-color laser scanning confocal microscope that was custom designed and built at AECOM specifically for the maximum sensitivity necessary to measure low abundance mRNAs. GenePix Pro 3.0 (Axon Instruments, Inc.) was used to generate raw data files containing measurements of signal and background fluorescence emissions of Cy3 and Cy5, respectively, for each element.

Quality Control, Data Analysis, and Statistics. Primary data were flagged using default parameters set in GenePix Pro 3.0 program. Normalization and data processing were performed as described previously (17, 18). Briefly, NSI of each spot in both channels (Cy5 as channel 1 and Cy3 as channel 2) was determined by subtracting the local background from signal intensity values and then subjected to log transformation. The overall intensity for each channel (I_{ch1} and I_{ch2}) was calculated by taking power of the average of the log of the NSI for all genes. The ratio of the overall intensity in channel 1 over that in channel 2 is calculated as $r = I_{ch1}/I_{ch2}$. The intensities for both channels were therefore balanced by multiplying the NSI of each spot in channel 2 by factor R. Under our experimental conditions, ratios of 1.6 and larger (up-regulated) or 0.6 and smaller (down-regulated) were chosen as significantly different gene expression levels between two samples hybridized to the same array spot (18). Genes showing consistent differential expression across replica arrays were extracted for further analysis. These genes were grouped on the basis of their function in cancer invasion and metastasis by searching PubMed, SwissProt database,[8] and Online Mendelian Inheritance in Man databases. Functional categories were correlated with cell behavior observed in the primary tumor and in culture.

QRT-PCR. To verify the data obtained from microarrays, QRT-PCR analysis of selected overexpressed and underexpressed genes (*ECM1, TIMP2, EGFR, Keratin 19, BMP1,* and *ZBP-1*) was performed by using the iCycler Apparatus (Bio-Rad) with sequence-specific primer pairs for all genes tested (see Supplemental Table 1 for primer sequences, amplicon size and melting temperature). Briefly, 5 μg of total RNA were converted into cDNA and used for the 40-cycle 3-step PCR in the iCycler apparatus. The SYBR Green PCR Core Reagents system (Perkin-Elmer Applied Biosystems) was used for real-time monitoring of amplification. Amplicon size and reaction specificity were confirmed by agarose gel electrophoresis. Each PCR reaction was repeated three times, and the median threshold cycle (C_T) values were used for analysis. Results were evaluated with iCycler IQ Real Time Detection System software (Bio-Rad).

Western Blots. MTLn3 and MTC cells were washed with ice-cold PBS before direct extraction in radioimmunoprecipitation assay buffer. Lysates were clarified by centrifugation, and protein concentrations were measured by bicinchoninic acid protein assay (Bio-Rad). Equal amounts of proteins were resolved by SDS-PAGE and transferred to nitrocellulose membrane. The membrane was blocked in 5% nonfat dried milk in Tris-buffered saline plus 1% Tween 20 and incubated with primary antibodies to ZBP-1 (Ref. 19; p62, a rabbit polyclonal antibody generated against full-length chicken ZBP-1), EF1-α (20), or Arp2/3 (Ref. 21; p34, a rabbit polyclonal antibody against Arp2/3 M_r 34,000 subunit) for 1 h, followed by incubation with appropriate conjugated secondary antibody for 1 h at room temperature. Immunoreactive bands were detected by chemiluminescence (New England Nuclear, Boston, MA), according to the manufacturer's instructions.

Differential Distribution of ZBP-1 in MTLn3 and MTC. The cells were propagated in serum and fixed and stained with anti-p62 antibody that detects ZBP-1. The tumors were grown in rats for 3 weeks after cell injection, and then they were surgically removed, sliced into approximately 1-mm slices, covered in OCT compound (Electron Microscopy Sciences), and frozen in isopentane on dry ice and ethanol. Then the tissue was cryosectioned into slices of 7–10 μm. Sections were fixed in 4% formaldehyde and stained with either anti-ZBP or anti-Arp 2/3 antibodies.

RESULTS

We have examined the motility of nonmetastatic and metastatic tumor cells in live primary tumors *in vivo*. Initial imaging was done using a conventional laser scanning pinhole confocal microscope (7, 8). Although confocal imaging can be effective in virtually eliminating out-of-focus light from thick objects, which is necessary for intravital imaging, this technique does nothing to alleviate another major problem of intravital imaging, phototoxicity. The technique of

[6] http://www.aecom.yu.edu/home/molgen/facilities.html.
[7] M. Dabeva, personal communication.
[8] http://ca.expasy.org/sprot/.

multiphoton excitation provides an elegant solution to the problem of phototoxicity by preventing unwanted out-of-focus excitation. Excitation is confined only to the optical section being observed (13, 22). The sample is illuminated with light of a wavelength that is approximately twice (or three times) the wavelength of the absorption peak of the fluorophore in use. In the case of GFP, which has an absorption peak at approximately 480 nm, 960 nm light can be used for excitation. Essentially no excitation of the fluorophore will occur at the 960 nm wavelength out of the plane of focus because this wavelength is thus far removed from GFP's peak excitation wavelength. In addition, no bleaching will occur, nor will phototoxic products be generated in the bulk of the sample. A high peak power laser source is used in pulses that are shorter than a picosecond so that the mean power levels are moderate and do not damage the specimen. With this source, the photon density only at the point of focus will be sufficiently high for significant numbers of two photon events to occur to generate fluorescence. Out-of-focus interference is eliminated simply because it is never generated.

Comparison of Conventional Confocal and Multiphoton Microscopes in Intravital Imaging of Intact Mammary Tumors

Comparison of the laser scanning confocal microscope with the multiphoton microscope for imaging of primary mammary tumors was done in live anesthetized rats with 2.5-week-old tumors (Fig. 1). In both imaging techniques, we found that GFP in the tumor cells is an excellent cytoplasmic volume marker that allows the entire cell outline to be defined *in vivo* in the living intact tissue (7, 8).

Fig. 1*A* shows two series of optical sections obtained by stepping at 12-μm intervals through a primary tumor in a live animal. The *left panels* were obtained with the conventional confocal microscope, and the *right panels* were obtained with the multiphoton microscope using an infrared laser and an external detector to avoid the confocal pinhole. Comparison of these two z-series demonstrates the superiority of the multiphoton microscope in penetrating deep within the live tissue to generate high-resolution confocal images. The greater depth of imaging of the multiphoton microscope compared with the confocal microscope is impressive when one considers that the z-series obtained with the multiphoton was started 36 μm inside of the primary tumor and not at the surface, the point at which the signal from the confocal microscope has fallen away. Hence, whereas the deepest useful image possible with the conventional confocal microscopy was $<$40 μm, we have obtained useful images from depths of up to 300 μm with the multiphoton microscope (Fig. 2*E*). In addition, signal:noise ratio does not fall off significantly throughout the z-series obtained with the multiphoton microscope.

Fig. 1*B* shows two series of optical sections identical to those in Fig. 1*A* but repeated to demonstrate the relative amount of bleaching occurring upon reexposure of the same optical planes to laser light. The confocal z-series (*left panels*) is significantly bleached by repeated imaging, whereas the multiphoton z-series (*right panels*) has usable signal: noise ratio at all depths. Therefore, the bleach rate is much less in the multiphoton microscope. In addition, these results demonstrate that with the imaging conditions used to document cell behavior in this study, bleaching does not affect the interpretation of time-lapse images.

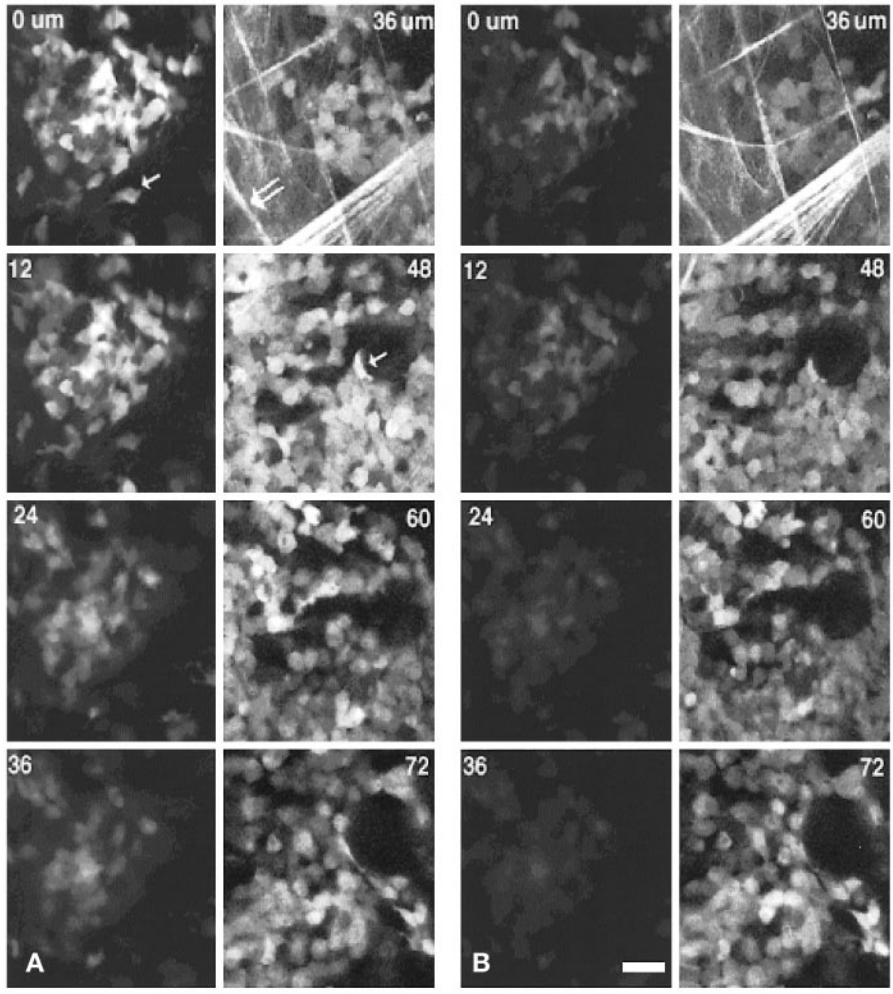

Fig. 1. Multiphoton microscopy is superior in imaging primary tumors more deeply and with less photodamage. *A*, initial z-series of images taken with the confocal (*left panels*) and multiphoton (*right panels*) microscope showing the greater depth of imaging possible with multiphoton excitation. The confocal microscope can only image to approximately 36 μm. The first panel of the multiphoton images (*top right panel*) begins at 36 μm and shows an image of better quality than that of the confocal image at 0 μm (*top left panel*). *Arrows* point to a single cell. *Double arrow* points to ECM seen only in multiphoton microscopy due to second harmonic generation. *B*, second z-series of the same focal planes illustrates dramatic improvement in GFP stability (*right panels*) in the multiphoton microscope compared with (*left panels*) the confocal microscope.

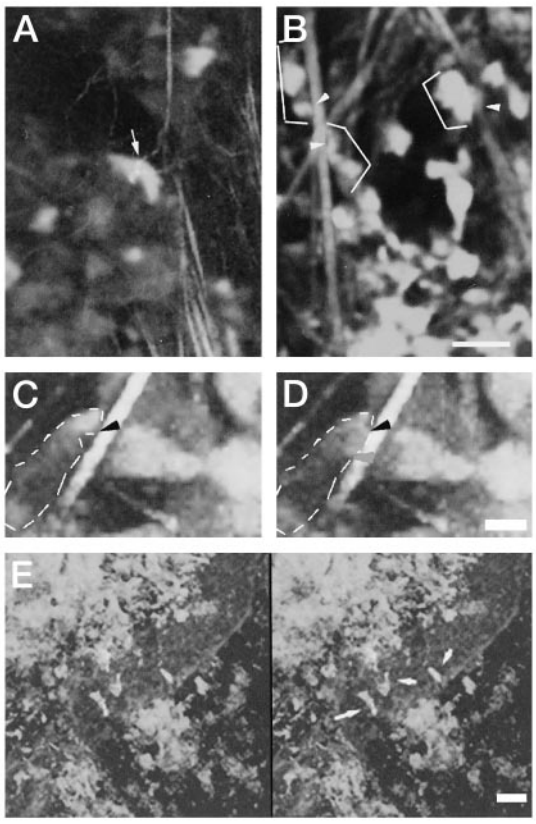

Fig. 2. Carcinoma cells in MTLn3 tumors adhere to ECM, extend pseudopods, and exhibit linear excursions toward blood vessels. Carcinoma cells in MTC (*A*) and MTLn3 (*B–E*) tumors were imaged by multiphoton microscopy. *A,* carcinoma cells in MTC tumors do not attach or orient on collagen-containing ECM fibers *in vivo*. A single fiber can be seen bending around the cell. The *arrow* points to collagen fiber bent over cell. *B,* carcinoma cells in MTLn3 tumors are observed to contact collagen-containing fibers. *Arrowheads* point to cell-matrix interactions. Elongated cells are highlighted by *brackets*. *Scale bar,* 25 μm. *C,* carcinoma cell is seen attached to matrix fiber (*black arrowhead* in *C*). The cell is delineated by the *white dotted line*. *D,* 4 min later, the carcinoma cell has spread along the fiber by approximately 8 μm. The *red arrowhead* shows the position of attachment after 4 min. The *black arrowhead* in *D* indicates the original attachment site in *C*. *Scale bar,* 10 μm. *E,* in a stereo pair image, GFP-labeled carcinoma cells are observed entering a rhodamine-dextran-filled blood vessel. The cells (*green*) are seen on the surface of the blood vessel (*red*) with pseudopodia (*yellow*) elongating into the vessel. *Arrows* point to cells entering blood vessel. The image is a 120-μm stack of 30 optical planes, each taken with a multiphoton microscope and then rendered as a stereo pair. The initial depth of the image is >100 μm. The blood space was labeled by injecting 2 M Dalton rhodamine-dextran i.v. into the blood space. *Scale bar,* 25 μm.

Differences in Carcinoma Cell Behavior in Metastatic and Nonmetastatic Primary Tumors

Intravital imaging of the behavior of cells in the MTC (nonmetastatic)- and MTLn3 (metastatic)-derived tumors demonstrates significant differences between the two. One of the advantages of multiphoton microscopy of intact tissue is the ability to image ECM-containing collagen by second harmonic generation (14, 23). As shown in Fig. 2, *A* and *B,* some carcinoma cells in MTLn3 tumors are closely associated with collagen fibers, whereas cells in MTC tumors do not associate. Rare interactions between carcinoma cells in MTC tumors and collagen fibers do not involve the movement of cells along the fiber, and the cells seem to push the fibers out of the way as they move (Fig. 2*A*). In metastatic MTLn3 tumors, the carcinoma cells move individually when in contact with collagen fibers (Fig. 2*B*, *arrowheads*). High-resolution time-lapse images of carcinoma cell movement on a collagen fiber are shown in Fig. 2, *C* and *D,* and they demonstrate the cell-collagen fiber interactions and linear locomotion exhibited *in vivo* by carcinoma cells in MTLn3 tumors. This result is consistent with the streaming like linear cell locomotion shown previously in MTLn3 tumors with conventional confocal microscopy (7). In these earlier studies, we were unable to see the underlying fibers that caused the linearity of motion.

The average instantaneous velocity of carcinoma cells from four different metastatic MTLn3 primary tumors was measured as 3.4 μm/min. However, in all of the tumors examined, it was apparent that only a small fraction of carcinoma cells in the primary tumor are actively motile during any given imaging interval. For some of these cells, instantaneous velocity values were close to the persistence value, indicating a high degree of rectilinear motion reminiscent of chemotaxis (15). The velocities of ~3.4 μm/min shown by carcinoma cells in the MTLn3 primary tumor are higher than the velocities exhibited by these cells in culture during either random motility (0.45 ± 0.08 μm/min, $n = 8$) or highly persistent motility (0.82 ± 0.19 μm/min, $n = 8$) observed in a gradient of EGF, which is chemotactic for these metastatic adenocarcinoma cells (24).

Carcinoma cells in MTC tumors move at rates similar to those in MTLn3 tumors, but the character of the cell motility is quite different. In MTC tumors, the cells move over each other, and the direction of motility is not linear and does not appear to be guided by collagen fibers (Figs. 2*A* and 4). The long linear excursions of carcinoma cells along collagen fibers and in association with vessels (Fig. 2, *C–E,* and Fig. 3) seen in MTLn3 tumors are not observed in MTC tumors (Fig. 4). There is no motility in MTLn3 tumors in areas where there are no vessels or collagen fibers. This is a major difference between the metastatic MTLn3 and nonmetastatic MTC tumors.

Differences in Intravasation by Carcinoma Cells in Metastatic and Nonmetastatic Primary Tumors

A strong correlation exists between the density of live carcinoma cells in the blood and the number of both single cells and metastases in the lungs, establishing intravasation as a key step for metastasis (8). Chemotaxis of carcinoma cells within the primary tumor toward growth factors such as EGF that are associated with blood vessels and

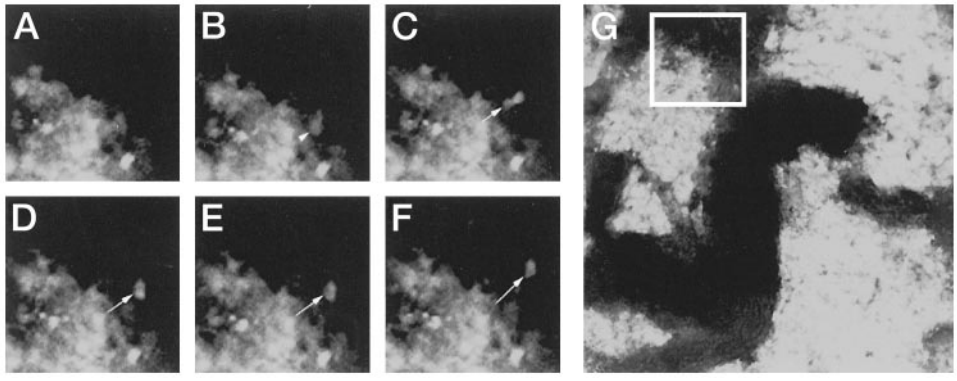

Fig. 3. Time-lapse imaging of intravasation of carcinoma cells in MTLn3 tumors. *A–F,* using multiphoton imaging, a single carcinoma cell (*green*) is seen crawling along a blood vessel. The *arrows* show the direction and the distance the cell moved along the vessel. Images were taken 5 min apart. *Scale bar,* 25 μm. *G,* the full field is shown to orient the area in which the cell in *A–F* is shown. Blood vessels are seen as *black areas* through carcinoma cell cords (*green*). The *white box* delineates the area seen in *A–F*.

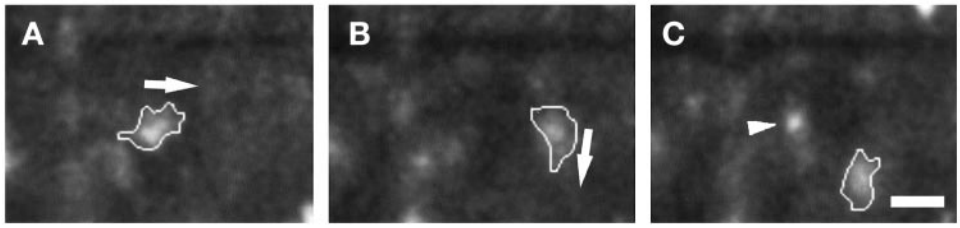

Fig. 4. Carcinoma cells in MTC tumors exhibit random motility with no relationship to either ECM or vessels. *A−C, white line* outlines the perimeter of a moving cell, whereas *arrows* show the direction of movement. Another cell is seen moving into the plane of focus C (*arrowhead*). Each frame is 4 min apart. *Scale bar,* 25 μm.

differences in the ability of carcinoma cells to resist lysis upon intravasation were proposed to be responsible for this correlation (8). Supporting chemotaxis are the observations of dramatic polarity of carcinoma cells toward blood vessels only in metastatic MTLn3 tumors and the high rates of chemotaxis of carcinoma cells measured within the primary tumor toward microneedles containing EGF and Matrigel (8, 25). To investigate the interaction of carcinoma cells with blood vessels in metastatic MTLn3 primary tumors in more detail and to determine if carcinoma cells have the intrinsic ability to locomote toward blood vessels and intravasate without fragmentation, we used GFP expression by carcinoma cells and multiphoton microscopy to time-lapse image the behavior of single carcinoma cells near blood vessels in the MTLn3 primary tumor. As shown in Fig. 2*E,* carcinoma cells are elongated and polarized toward blood vessels, suggesting that there is a vessel-mediated attraction for the cells. The depth of imaging possible with the multiphoton microscope illustrates, in the three-dimensional projection in Fig. 2*E*, that many of the carcinoma cells cross the vessel wall as intact single cells. That this is an active process requiring each cell to cross an intact vessel wall is shown by the failure of i.v. injected low molecular weight fluorescent dextran to escape from the vessels during intravasation (Fig. 2*E*). Furthermore, time-lapse imaging of cells in contact with blood vessels demonstrates the ability of carcinoma cells to actively crawl into the blood vessel using amoeboid locomotion (Fig. 3). Finally, fragmentation of carcinoma cells, as observed in MTC tumors during intravasation (8), was not observed in metastatic MTLn3 tumors. All of these results correlate directly with the large number of GFP-expressing carcinoma cells observed in the circulation of the MTLn3 primary tumors (Fig. 5) and their absence from the vessels of MTC tumors (8).

Differences in ECM between Metastatic and Nonmetastatic Primary Tumors

To estimate the amount of ECM present in the primary tumor, we used second harmonic generation to image collagen fibers in the primary tumor *in vivo* (14, 23). As shown in Fig. 6, the amount, integrity, and size of the collagen fibers in the second harmonic image were reduced in MTLn3 compared with MTC tumors. As shown in Fig. 6*C,* metastatic MTln3-derived tumors have 2.4 times less collagen than MTC tumors. This is consistent with the general observations that the MTC tumors are more fibrous and less necrotic and that the clusters of carcinoma cells in MTC tumors are far apart due to intervening large collagen arrays (Figs. 2 and 6). However, as shown in Fig. 1, large amounts of collagen are observed near the outside edge of MTLn3-generated tumors, where the cells are seen adhering to and elongated on the collagen fibers.

Summary of Behavioral Differences

Based on the multiphoton microscope observations reported here and on previous studies with the same tumor models (8, 25), there are five major differences in cell behavior between the MTLn3- and MTC-derived primary breast tumors: (*a*) in MTLn3 tumors, some carcinoma cells are associated with collagen fibers, whereas in MTC tumors, this is not observed; (*b*) linear cell motility is seen along collagen fibers in MTLn3 tumors; (*c*) there is increased carcinoma cell polarity and locomotion toward blood vessels in metastatic MTLn3 tumors, whereas carcinoma cells in MTC tumors appear oriented toward each other, but not toward vessels; (*d*) carcinoma cells in MTLn3 tumors remain intact during intravasation, whereas carcinoma

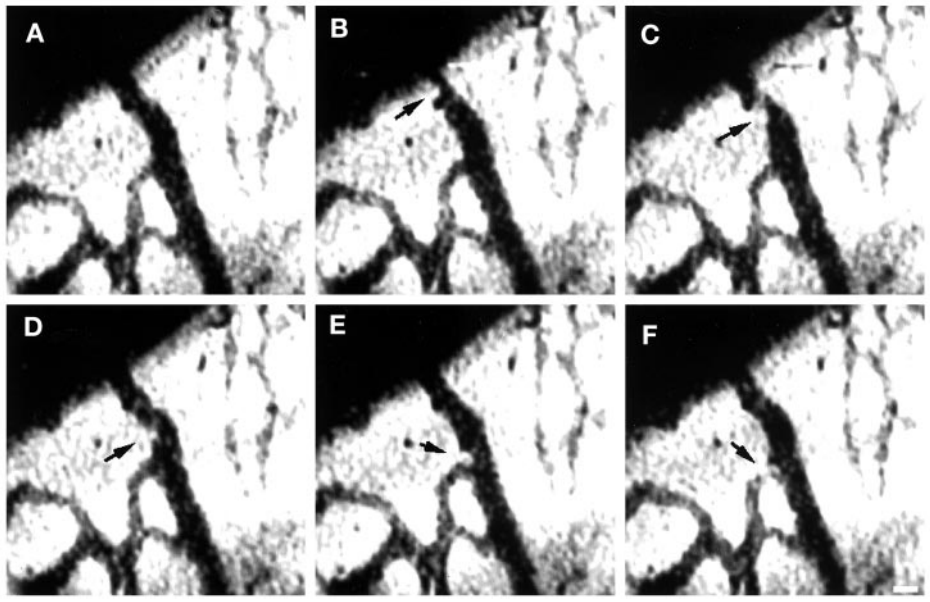

Fig. 5. Intact GFP-expressing carcinoma cells are routinely observed in the circulation of MTLn3 primary tumors. A GFP-labeled carcinoma cell can be seen rolling down the side of a vessel. The vessels are imaged by contrasting the vessels against the fluorescent tumor using a SIT camera and capturing frames at 30 frames/s. The cell moves through the vessel at 3.3 μm/s. Carcinoma cells are seen in blood vessels 6-fold more often in MTLn3 tumors than in nonmetastatic MTC tumors, appearing at a rate of 2.2 ± 0.72 cells/min in MTLn3 as compared with 0.34 ± 0.13 cells/min for MTC tumors. *Scale bar,* 25 μm.

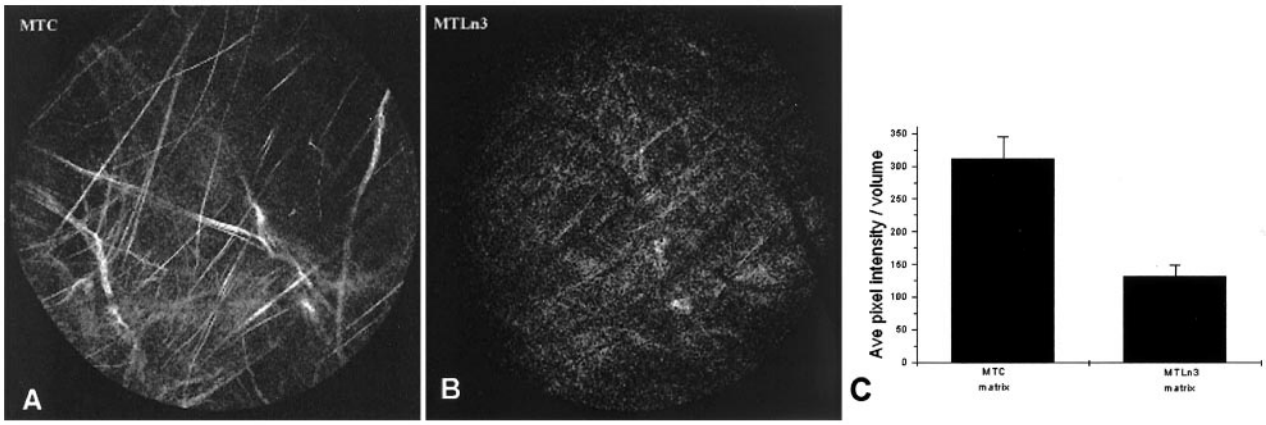

Fig. 6. MTC tumors have more collagen-containing ECM than MTLn3 tumors. By imaging the second harmonic signal of ECM using multiphoton microscopy, the difference in collagen content between the two tumor types was determined. *A*, MTC tumors at 35 μm depth into the tumor can be seen to have more matrix than (*B*) MTLn3 tumor at the same depth of focus. The images were collected through a blue/green dichroic with a wavelength cutoff below 500 nm, so only the second harmonic signal was collected. The tumors used to generate these images did not contain GFP to avoid stray fluorescence. *C*, by calculating the pixel intensity for the captured volume of a z-series of each tumor, MTC tumors are seen to have on average of 2.4 times more matrix than MTLn3-generated tumors. $n = 4$. The laser power and photomultiplier tube gain were constant for all measurements.

cells in MTC tumors fragment; and (*e*) collagen fiber density is higher in MTC tumors. These behavioral differences predict seven categories of molecular differences between metastatic and nonmetastatic tumors as follows: (*a*) ECM composition; (*b*) adhesion molecules; (*c*) cytoskeleton involved in motility; (*d*) mechanical stability and survival; (*e*) cell polarity; (*f*) chemotaxis toward vessels; and (*g*) proteolysis of collagen.

Identification of Differentially Expressed Genes in Metastatic and Nonmetastatic Primary Tumors and Their Progenitor Tumor Cells

To obtain a profile of differential gene expression that is associated with the behavioral differences observed between MTLn3- and MTC cell-derived primary tumors, whole primary tumors were isolated from host animals and subjected to cDNA microarray analysis on 9700 gene arrays. We also studied the cultured cells from which the primary tumors were derived because they are a more homogeneous cell population than whole tumors (24). Comparative differential gene expression analysis of metastatic and nonmetastatic tumors and their progenitor cells in culture revealed only 161 genes with differential expression patterns in both tumors and their progenitor cells in culture. Supplemental Table 2 shows the complete list of differentially expressed genes. Of these, 119 genes are more highly expressed (at least 1.6×) in MTC compared with MTLn3 tumors, and 42 genes are more highly expressed (at least 1.6×) in MTLn3 compared with MTC tumors. Among the genes with known functions, at least 70 of them (shown in bold in Supplemental Table 2) are known to be involved in cancer invasion and metastasis. In addition, 61 expressed sequence tags of unknown function also showed different patterns of expression. To relate cell behavior to gene expression, in this study we therefore focused on the genes of known function and related them to each of the behavioral phenotypes seen *in vivo*.

Validation of Array Data by QRT-PCR

We verified the array results using real-time PCR for selected genes. As shown in Fig. 7, in general, most genes showed the same pattern of expression with both array and real-time PCR. However, studies have shown that fluorescent dye-based microarrays can be less sensitive than the PCR-based differential display method in detection of low abundance mRNA species (26). One of these mRNAs, ZBP-1, which regulates cell polarity by targeting mRNA to the leading edge, has been shown to be overexpressed in most tumors and can be used as a novel human tumor marker (27–29). Our microarrays detected larger differences in culture than in the primary tumors in ZBP-1 expression, whereas real-time PCR reproducibly showed a large increase in expression in both cultured MTC cells and whole MTC tumors.

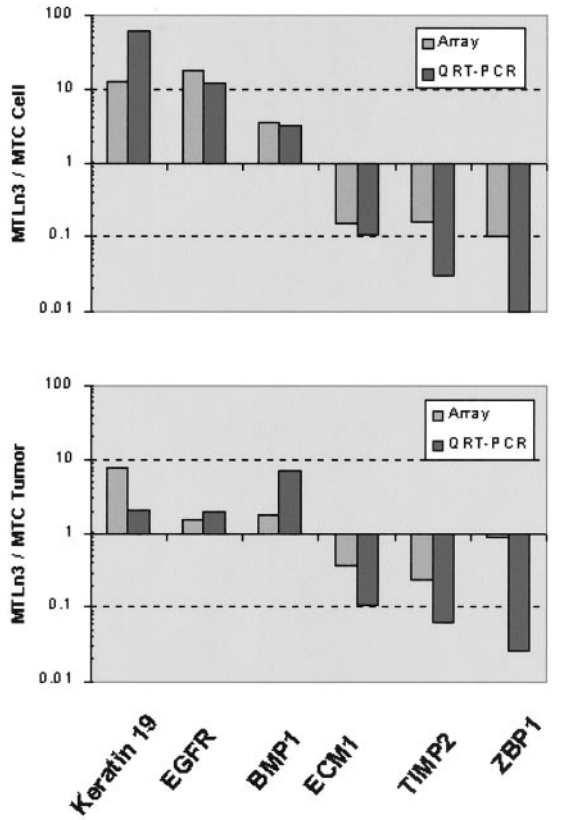

Fig. 7. Validation of microarray results for selected genes by QRT-PCR. Comparison of expression analyses in cells in culture (*top panel*) and whole tumors (*bottom panel*) gives similar results for cDNA microarrays and QRT-PCR, except for low abundance mRNAs such as ZBP-1.

Correlation of Cell Behavior with Gene Expression Patterns

Imaging of cell behavior within the tumor provided a way to interpret the cDNA microarray analyses. In this approach, genes with different expression patterns and known cellular functions were divided into seven categories of genes predicted from the behavior of carcinoma cells *in vivo* (Table 1).

ECM Composition. A major behavioral difference between MTC and MTLn3 tumors is the abundance of collagen fibers in MTC tumors. Consistent with this is the overexpression of several collagen genes involved in ECM assembly (*Col3a1, Col5a2,* and *Col6a3*) in MTC tumors and cells in culture (Table 1).

Two laminin genes, *Lama5* and *Lamc2*, are found to be differentially expressed in these two tumor types. *Lama5*, encoding laminin α-5, is more highly expressed in MTC cells and tumors. *Lamc2* gene, encoding laminin-5 γ2 chain, is found to be more highly expressed in MTLn3 tumors and cells in culture (Table 1). The laminins are components of basement membranes that are believed to act as a mechanical barrier against carcinoma cell invasion (4). Laminin-5 is also reported to stimulate cell migration after proteolysis. Two other genes highly expressed in MTC tumors and cells are *Ecm1* encoding ECM protein 1 and *Comp* encoding cartilage oligomeric matrix protein (Table 1).

Adhesion Molecules. In the category of adhesion molecules, both E-cadherin and P-cadherin show much higher expression in MTLn3 cells and tumors (Table 1). MTLn3 tumors and cells also express more of tight junction protein 2, a protein that may play a critical role in cell-cell adhesion (30). Two other major adhesion molecules, CD151 and Adam19, were found to be highly expressed in MTC tumors and

Table 1 *List of genes that are differentially expressed and correlated with cell behavior in MTLn3 and MTC tumors*

Gene functions are based on NCBI PubMed, SwissProt data base (http://ca.expasy.org/sprot/) and Online Mendelian Inheritance in Man (*http://www.ncbi.nlm.nih.gov/omim/*). NC, no change detected by array. Numbers in parentheses indicate the changes detected by QRT-PCR.

Gene names organized by gene function	GenBank accession no.	Protein	Mean MTLn3:MTC (culture)	Mean MTLn3:MTC (tumor)
ECM composition				
Col3a1	W89883	Collagen, type III, α 1	0.01	0.15
Col5a2	AA034564	Collagen, type V, α 2	0.05	0.19
Col6a3	W16221	Collagen, type VI, α 3	0.22	0.11
Lamc2	W49392	Laminin, γ 2	4.23	1.74
	W09048	Laminin, γ 2	3.18	1.96
Lama5	AA049251	Laminin, α 5	0.52	0.53
Ecm1	AA474897	ECM protein 1	0.09	0.37
Comp	AA064293	Cartilage oligomeric matrix protein	0.31	0.60
Adhesion molecules				
Cdh3	W12889	Cadherin 3, P-cadherin	9.19	3.00
Cdh1	AA276110	Cadherin 1, E-cadherin	9.82	3.31
Tjp2	W91219	Tight junction protein 2	2.96	2.16
Cd151	AA050218	CD151 antigen	0.16	0.29
Adam19	AA138786	A disintegrin and metalloproteinase domain 19	0.13	0.41
Cytoskeleton involved in motility				
EST	W47753	AR16_Human ARP2/3 complex M_r 16,000 subunit	6.31	5.45
Cappa1	AA414612	Capping protein 1	NC	2.65
Cttn	W96939	Cortactin	0.23	0.58
Pfn2	AA139628	Profilin 2	0.22	0.35
Rock2	AA098168	Rho-associated coiled-coil forming kinase 2	NC	2.13
Mechanical stability and survival				
Krt1-19	AA028346	Cytokeratin 19	12.30	7.97
Krt1-13	AA080232	Cytokeratin 13	NC	2.79
Krt2-1	W63927	Keratin complex 2, basic, gene 1	0.24	0.43
Rab25	AA538228	Member Ras oncogene family	7.99	6.38
Rab19	AA118762	Member Ras oncogene family	2.26	1.66
Bcl2l10	AA426964	BCL2-like10	NC	3.07
Met	AA212170	Met proto-oncogene	2.55	1.96
EST	AA471761	Cellular apoptosis susceptibility protein	0.62	0.64
Pdcd	AA465936	Programmed cell death 4	0.30	NC
Cell polarity				
Zbp1(crdbp)	AA073514	Zip code-binding protein 1	0.08	NC (0.027)
Stau1	AA270608	Staufen	0.48	NC
Eef1a1	AA259551	EF1-α	NC	2.69
Chemotaxis toward vessels				
Egfr	AA237224	EGFR	20.12	NC (2.0)
EST	AA059642	EGFR-pathway-substrate 8, EPS8	NC	2.77
Cav	AA138693	Caveolin, caveolae protein, M_r 22,000	0.04	0.17
Pak1	AA061378	PAK1 serine/threonine kinases	0.28	0.53
Mapk7	AA395937	Mitogen-activated protein kinase 7	0.57	0.39
Fgfr1	AA272097	FGF receptor 1	0.32	0.35
Igfbp5	AA241784	IGF-binding protein 5	0.15	0.14
Lef1	AA119479	Lymphoid enhancer-binding factor 1	0.11	0.26
Gpcr26	W97046	G-protein-coupled receptor 26	0.14	0.20
Gtr2	W70912	Small GTPase	0.46	0.45
Tbk1	AA475369	TANK-binding kinase TBK1	0.45	0.52
EST	AA049480	Bone morphogenetic protein 3 precursor	0.06	0.44
	W13196		0.04	0.35
Spp1	AA108928	Secreted phosphoprotein 1, also as osteopontin (OPN)	0.03	0.07
9-sep	W33661	Septin 9	0.18	0.42
Proteolysis of collagen				
Bmp1	W82677	Bone morphogenetic protein 1	3.49	1.72
Spi4	AA218279	Serine protease-inhibitor 4	0.03	0.11
Timp2	AA444490	Tissue inhibitor of metalloproteinase 2	0.16	0.19
Cst3	W78651	Cystatin 3	0.08	0.22
Mmp2	W80177	Matrix metalloproteinase 2	0.03	0.15

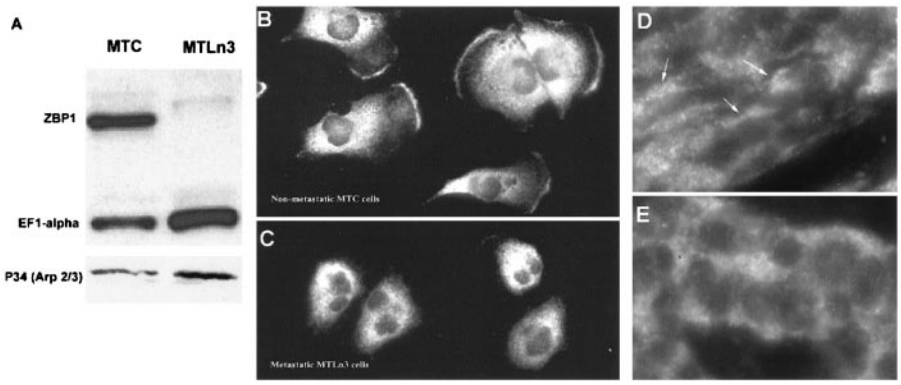

Fig. 8. ZBP-1, EF1-α, and Arp2/3 are differentially expressed at the protein level in MTLn3 and MTC cells. ZBP-1 is localized to the polarized leading edge of carcinoma cells in MTC tumors. Whole cell extracts from MTLn3 and MTC cells were resolved by SDS-PAGE and subjected to immunoblotting with polyclonal antibodies against either ZBP-1, EF1-α, or Arp2/3 p34 subunit to detect their expression at the protein level. ZBP-1 shows higher expression in MTC cells (MTC:MTLn3 ratio $>$ 13), whereas EF1-α (MTLn3:MTC ratio = $\sim$1.5) and Arp2/3 p34 (MTLn3:MTC ratio = $\sim$2) show more expression in MTLn3 cells. MTC cells (*B*) and MTLn3 cells (*C*) were fixed and stained with anti-p62 antibody that detects ZBP-1. ZBP-1 is localized to the leading edge of MTC cells, whereas MTLn3 cells show a diffuse distribution. MTC tumors (*D*) and MTLn3 tumors (*E*) were grown in rats for 3 weeks and then surgically removed, cryosectioned, and stained with anti-p62 antibody that detects ZBP-1. Note the polarized distribution of ZBP-1 to one pole of each cell only in carcinoma cells of MTC tumors (*arrows*).

cells (Table 1). Transmembrane 4 superfamily protein CD151 associates with β_1 and $\alpha_{IIb}\beta_3$ integrins in hemopoietic cell lines and modulates cell-cell adhesion (31). Adam19/adamalysin-19 (a disintegrin and metalloproteinase) is involved in proteolysis, adhesion, fusion, and intracellular signaling (32).

Cytoskeleton Involved in Motility. Microarray analysis shows that the M_r 16,000 subunit of the Arp2/3 complex is greatly overexpressed in MTLn3 cells and tumors (Table 1). Because the p16 subunit is the only Arp2/3 component spotted on the array, we tested the expression level of subunit p34, a marker for the Arp2/3 complex (33), at the protein level using Western blotting. These results indicate that MTLn3 cells express at least 2-fold more p34 at the protein level (Fig. 8*A*). Capping protein is more highly expressed in MTLn3 tumors, but not cells (Table 1). Capping protein caps the barbed ends of actin filaments to regulate actin dynamics (34).

Another gene highly expressed in MTLn3 tumors is *ROCK2* (Table 1). ROCK2, an isozyme of ROCK1, is a direct downstream target of Rho (35).

Cortactin is involved in stimulating the binding of activated Arp2/3 complex to the sides of actin filaments to decrease debranching (36). Unlike the Arp2/3 complex, cortactin was more highly expressed in MTC cells and tumors (Table 1).

Profilin was also more highly expressed in MTC cells and tumors (Table 1). Profilin increases the on-rate of actin monomers at the barbed end sufficiently to lower the critical concentration for actin polymerization (34).

Mechanical Stability and Survival. MTLn3 cells and tumors exhibit dramatic overexpression of keratins 19 and 13, whereas MTC cells and tumors express a higher level of keratin complex 2 (Table 1). In addition, the array data show that MTLn3 cells and tumors express more apoptosis suppressors such as Rab19, Rab25, BCL2l10, and Met (37). Also consistent with cell fragmentation in MTC tumors, MTC cells and tumors express more programmed cell death and cellular apoptosis susceptibility proteins such as Pdcd and Casp (cellular apoptosis susceptibility protein).

Cell Polarity. ZBP-1 and staufen expression in MTLn3 cells was much lower compared with MTC cells in culture (Table 1). To detect differences in expression of this low abundance message in tumors, QRT-PCR was used for ZBP-1 as described above and shown in Fig. 8. A very large overexpression of ZBP-1 was demonstrated in both MTC cells and tumors compared with MTLn3 samples. ZBP-1 is a RNA-binding protein that binds to the mRNA zip code and functions to localize β-actin mRNA (19). Mammalian Staufen is a double-stranded RNA-binding protein potentially involved in mRNA transport and localization (38).

To confirm the increased expression of ZBP-1 at the protein level in MTC cells and tumors, immunohistochemistry was performed using anti-ZBP-1 antibody in both cultured cells and tumors. The pixel intensity showed that in cultured cells, MTC cells and carcinoma cells in MTC-generated tumors express more ZBP-1 compared with MTLn3 cells. Western blots also showed that MTC cells express 13-fold more ZBP-1 than MTLn3 cells (Fig. 8*A*). In addition, as shown in Fig. 8, *B–E,* ZBP-1 was found to be polarized in MTC cells in culture and in carcinoma cells within the primary tumor, whereas ZBP-1 was diffusely distributed in both MTLn3 samples.

A related protein, EF1α, was found to be more highly expressed in MTLn3 cells (Table 1), which is consistent with its overexpression at the protein level in MTLn3 cells (20). EF1α is an elongation factor that is involved in mRNA anchorage at the leading edge in polarized cells, and its overexpression in correlated with delocalization of mRNA (39).

Chemotaxis toward Vessels. Another major behavioral difference was chemotaxis to EGF of MTLn3 cells but not MTC cells as observed both in culture and in tumors (24, 25). Consistent with this, expression data showed significant differences in the expression of genes encoding chemotaxis and signal transduction molecules that are known to play roles in cancer invasion and metastasis (Table 1). The high level of EGFR in MTLn3 cells is consistent with previous studies (40). EGFR signaling involves small GTPases of the Rho family, and EGFR trafficking involves small GTPases of the Rab family. Lanzetti *et al.* (41) reported that the EPS8 (EGFR pathway substrate 8) protein coordinates EGFR signaling through Rac and trafficking through Rab5. We detected 3-fold more expression of EPS8 in MTLn3 tumors compared with MTCs.

Array analysis shows that caveolin is highly expressed in MTC cells and tumors (Table 1). Caveolin-1 is a principal component of caveolae membranes and may function as a tumor suppressor. Interestingly, MTLn3 cells fail to express detectable levels of endogenous caveolin-1. In a recent study (42), an inducible adenoviral gene delivery system was used to achieve tightly controlled expression of caveolin-1 in MTLn3 cells. Caveolin-1 expression in MTLn3 cells inhibits EGF-stimulated lamellipod extension and cell migration and blocks anchorage-independent cell growth. This result suggests that caveolin-1 expression in MTC cells causes a nonmotile phenotype.

PAK1, which is more highly expressed in MTC tumors and cells (Table 1), promotes the disassembly of stress fibers and focal adhesions. PAKs may regulate cytoskeletal dynamics by decreasing myosin light chain kinase activity and myosin light-chain phosphorylation (43).

Other signaling genes more highly expressed in MTC tumors and cells (Table 1) are genes encoding FGF (*FGF*), IGF-binding protein 5 (*IGFBP5*), mitogen-activated protein kinase 7, lymphoid enhancer factor 1 (*Lef1*), G protein-coupled receptor 26 (*Gpcr26*), glutamyl-tRNA reductase 2 (*Gtr2*), Tank binding kinase (*Tbk1*), and bone morphogenetic protein 3 (*Bmp3*). They are documented to be involved in different signaling pathways. *Spp1*, the gene encoding secreted phosphoprotein 1, a phosphorylated glycoprotein with diverse functions in cell adhesion and chemoattraction, is highly expressed in MTC tumors and cells (Table 1). Septin 9 is also highly expressed in MTC samples. It is implicated in a variety of cellular functions involving specialized regions of the cell cortex and changes in cell shape.

Proteolysis of Collagen. MTLn3 cells express much more BMP1 than MTC (Table 1). The *BMP1* locus encodes a procollagen C proteinase, a secreted metalloprotease requiring calcium (44, 45). A recent study (45) found that BMP1 cleaves the laminin-5 (LAMA3) chain at sites within the G4 subdomain and the IIIa domain and that BMP1 cleaves the LAMC2 chain within the second EGF-like repeat of domain III. Consistent with the observation of more intact collagen in MTC tumors is the finding that Spi4, Cst3, and TIMP2, all inhibitors of proteinases, are overexpressed in MTC cells and tumors compared with MTLn3 samples (Table 1). TIMP 2, a M_r 21,000 protein that is secreted by melanoma cells and binds to type IV collagenase proenzyme secreted by the same cells, has been shown to block tumor cell invasion both *in vitro* and *in vivo*, suggesting that it acts as metastasis suppressor gene. However, Mmp2 encoding matrix metalloproteinase-2 (MMP2 or type IV collagenase, M_r 72,000), is also highly expressed in MTC tumors and cells (Table 1).

DISCUSSION

The Interaction of Carcinoma Cells with ECM. Carcinoma cells in metastatic MTLn3 tumors are associated with and locomote on collagen-containing fibers, whereas this is not seen in MTC tumors. This suggests that either adhesion molecules mediating the attachment of carcinoma cells to collagen-containing ECM are different or the signals for cell adhesion and motility associated with collagen-containing fibers are different between MTC and MTLn3 tumors. The array analysis did not detect any large differences in integrin receptor expression, which is inconsistent with the first possibility.

A large increase in cadherin expression was found in MTLn3 tumors and cells. Cadherins are a family of calcium-dependent adhesion molecules involved in cell-cell aggregation and epithelial formation. Dysfunction of the cadherin pathway is involved in tumor invasiveness and disease progression for a variety of carcinomas (46). High levels of cadherin expression have been correlated with loss of cell-cell adhesion when proteolysis of the extracellular domain of cadherin generates peptides that disrupt the homotypic cadherin interaction on neighboring cells leading to invasion (47). The high levels of expression of proteases and low levels of expression of TIMPs in MTLn3 tumors are consistent with this possibility. In ovarian carcinoma cells of epithelial origin, cadherin expression promotes invasion, presumably by providing the adhesion and traction required for migration (48).

Collagen expression was lower, and collagen content, as measured by second harmonic generation, was significantly reduced in MTLn3 tumors. This latter observation is correlated with the higher levels of proteinase expression and lower levels of proteinase inhibitor expression in MTLn3 tumors compared with MTC tumors, suggesting significantly more proteolysis of ECM in MTLn3 tumors. These observations are consistent with the possibility of a large difference in signals for adhesion and motility in association with collagen fibers between MTLn3 and MTC tumors because proteolytic products of collagen are well known to stimulate adhesion and cell motility in culture (24). Chemotaxis to fragments of ECM has also been reported (4), suggesting that proteolysis in the local cell environment may elicit directional cell motility along ECM fibers as observed in MTLn3 tumors.

To invade, carcinoma cells need to penetrate through the basement membrane and remove ECM tissue boundaries (4). In this context, proteases are believed to play a key role because they can either degrade or process the ECM components and thereby support invasion and intravasation. The pattern of proteinase production and relative lack of proteinase inhibitors in MTLn3 tumors support the observed increase in invasion and intravasation in live animals.

Polarity and Chemotaxis of Carcinoma Cells toward Blood Vessels. One of the most remarkable observations made in live tumors both here and in previous studies was the dramatic polarization of carcinoma cells toward blood vessels in metastatic MTLn3 tumors (8). This was correlated with large differences in chemotaxis toward locally applied EGF in the primary tumor (25), increased blood burden of carcinoma cells in MTLn3 tumors as shown here, and metastatic efficiency (8), indicating that chemotaxis to blood vessels could increase the efficiency of intravasation and metastasis. Cell polarity and chemotaxis toward vessels could be induced by chemoattractant diffusing from the blood vessel. Growth factors including EGF, platelet-derived growth factor, FGF, and IGF are present in serum, macrophages, platelets, and smooth muscle cells associated with vessels (49–52). Release of growth factors from these cells or endothelial cells could provide a gradient that would produce a chemotactic response. Both our array data and results from other groups (40) demonstrate that MTLn3 cells express more EGFRs than MTC cells, and the data reported here show a significantly greater expression in MTLn3 tumors. However, MTC cells and tumors express much higher levels of FGF receptor and IGF-binding protein than MTLn3 cells and tumors. This suggests that chemotaxis toward vessels is specific to EGF because carcinoma cells in MTC tumors do not polarize and chemotax toward vessels. Experimental expression of the EGFR in MTC cells increases chemotactic responses to EGF *in vitro* and metastatic ability *in vivo* (9, 53, 54). Expression of the EGFR and its homologues, such as ErbB-2, has been correlated with poor prognosis in human breast tumors (55). Finally, chemotaxis to EGF has been demonstrated within MTLn3 primary tumors using microneedles containing Matrigel and EGF (25). Therefore, chemotaxis to blood vessels, mediated by the EGFR, is important in enhancing metastatic capability in addition to the well-characterized effects of EGFR signaling on mitogenesis.

Another positive correlation resulting from the comparison of cell behavior and expression analysis is the relationship between cell polarity and chemotaxis toward blood vessels. As reported previously (8, 12), metastatic primary tumors contain carcinoma cells that form loose clusters of rounded, nonpolarized cells except near blood vessels, where they are highly polarized toward vessels. Nonmetastatic primary tumors contain carcinoma cells with intrinsic polarity that are elongated and polarized in tight sheets regardless of the presence or absence of blood vessels. This was confirmed by examination of both the histopathology and intravital images of tumors (7, 8, 12, 25). Furthermore, the polarity of carcinoma cells in MTC tumors is closely correlated with the intrinsic polarity of the MTC cells in culture,

which exhibit polarized crawling, whereas MTLn3 cells do not exhibit intrinsic polarity and undergo random walking in culture (12).

A key difference between these cells that may explain the difference in intrinsic polarity is the targeting of mRNA for β-actin to the leading edge. In the array data reported here, MTC cells express much more ZBP-1, and this was confirmed at the protein level by Western blotting and immunohistochemistry. ZBP-1 is polarized at the cell pole in MTC cells in culture and in tumors, whereas it is diffuse in MTLn3 samples. This is correlated with the failure of MTLn3 cells to target β-actin mRNA to the leading edge and the failure to develop intrinsic polarity resulting in random walking (12). The mechanism relating mRNA targeting to the leading edge and intrinsic cell polarity involves the localization of β-actin nucleation to the leading edge during motility. Disruption of mRNA targeting to the leading edge using oligonucleotides that disrupt the interaction between ZBP-1 and the targeting sequence in the mRNA, the zipcode, results in delocalization of mRNA and β-actin nucleation sites and the disruption of cell polarity (56). The overexpression of ZBP-1 in MTC cells relative to MTLn3 cells is consistent with the higher level of intrinsic cell polarity of MTC cells in culture and in tumors. In general, cells that lack a fixed intrinsic polarity are more chemotactic to exogenous gradients presumably because there is no intrinsic polarity to be overcome by the exogenous chemotactic signal (12, 25, 56). This might explain why MTLn3 cells, with relatively low expression of ZBP-1 and no intrinsic polarity, were more polarized in a chemotactic field near blood vessels.

Cell Motility. A major difference between the motility of carcinoma cells in MTC and MTLn3 tumors is the local and nonlinear movement of cells in MTC tumors compared with the long linear excursions of carcinoma cells along collagen fibers and toward blood vessels seen in MTLn3 tumors. This is quite different from the motility of these cells in culture, where MTC cells exhibit linear crawling compared with the random walking of MTLn3 cells. This apparent reversal of behavior suggests that the motility of carcinoma cells in MTLn3 tumors is dominated by chemotaxis signals emanating from the processing of ECM and by chemoattractants associated with blood vessels. In addition, our array data suggest additional differences between MTC and MTLn3 cells in the expression of key proteins involved in leading edge dynamics that might contribute to enhanced chemotaxis ability.

Two functionally related proteins that are overexpressed in MTLn3 tumors and cells are the Arp2/3 complex and capping protein. The Arp2/3 complex is an EGFR-linked actin nucleation complex in the leading edge that nucleates actin filaments to elongate against the cell membrane to form lamellipods (33, 57). This event determines cell polarity in response to EGF stimulation and is a key first step in chemotaxis (24, 33). The greatly increased expression of Arp2/3 complex in MTLn3 cells is expected to significantly enhance chemotaxis of carcinoma cells in MTLn3 tumors and in culture because inhibition of the nucleation activity of Arp2/3 complex in carcinoma cells inhibits chemotaxis to EGF (33). In addition, the higher expression of capping protein in MTLn3 tumors is expected to greatly enhance the efficiency of nucleation by Arp2/3 complex (34).

A functionally related protein that is overexpressed in MTC cells and tumors is cortactin. Cortactin is tyrosine phosphorylated in response to FGF and EGF in fibroblasts (58) (59) and binds to Arp2/3 complex and stimulates its nucleation activity weakly but strongly stabilizes Arp2/3-mediated filament branches (36). The relative overexpression of cortactin in MTC cells and tumors reported here is consistent with the higher level of intrinsic polarity of carcinoma cells in MTC tumors and in culture, where the stabilizing effect of cortactin on the actin network at the leading edge could stabilize cell polarity.

Mechanical Stability and Survival during Intravasation. The majority of tumor cells that enter the circulation are rapidly eliminated by the immune system or apoptosis. Fibrin deposits, platelet aggregation, and cell adhesion in tumor emboli may protect circulating cells from mechanical trauma, facilitate their arrest in capillary beds, and protect tumor emboli from destruction by host immunity (60). From our array data, we have found that carcinoma cells in MTLn3 tumors and culture highly express laminins and cadherins and apoptosis suppressor genes, all of which may contribute to survival in the circulation. In contrast, carcinoma cells in MTC tumors and culture express genes involved in programmed cell death at higher levels. The combination of these factors may contribute to the increased numbers of viable carcinoma cells in the circulation of MTLn3 tumors.

A novel observation resulting from intravital imaging of these tumors is the dramatic fragmentation of carcinoma cells when in contact with blood vessels in MTC tumors (8) compared with the ability of carcinoma cells in MTLn3 tumors to enter blood vessels as intact whole cells as shown here. A potential explanation for this difference in behavior is the large relative overexpression of cytokeratins by carcinoma cells in MTLn3 tumors. These keratins form the largest subfamily of intermediate filament proteins and play critical roles in the mechanical stability of epithelial cells subjected to shear forces (61).

In conclusion, we have developed animal models of breast cancer that allow the direct examination of the behavior of individual GFP-expressing carcinoma cells in live nonmetastatic and metastatic primary tumors *in situ*. When combined with multiphoton microscopy to image differences in cell behavior, insights into the microenvironment of carcinoma cells in the primary tumor can be obtained. When correlated with results from cDNA microarray analyses, the behavioral insights allow the identification of potentially important genetic determinants for breast cancer invasion and metastasis. We conclude that aligning cell behavior *in vivo* with patterns of gene expression can lead to the molecular mechanisms behind invasion and metastasis.

ACKNOWLEDGMENTS

We gratefully acknowledge Dr. Jeffrey W. Pollard for critical reading and valuable discussion of the manuscript. We also thank Dr. Weijia Zhang for help with microarray analysis. We are grateful to Aldo Massimi (AECOM Microarray Core) and members of the Analytical Imaging Facility for support and advice. We thank Dr. Mariana Dabeva of the AECOM Liver Center for advice about using mouse cDNA arrays.

REFERENCES

1. Fidler, I. J. Critical determinants of cancer metastasis: rationale for therapy. Cancer Chemother. Pharmacol., *43:* S3−S10, 1999.
2. Morris, V. L., Schmidt, E. E., MacDonald, I. C., Groom, A. C., and Chambers, A. F. Sequential steps in hematogenous metastasis of cancer cells studied by *in vivo* videomicroscopy. Invasion Metastasis, *17:* 281–296, 1997.
3. Naumov, G. N., Wilson, S. M., MacDonald, I. C., Schmidt, E. E., Morris, V. L., Groom, A. C., Hoffman, R. M., and Chambers, A. F. Cellular expression of green fluorescent protein, coupled with high-resolution *in vivo* videomicroscopy, to monitor steps in tumor metastasis. J. Cell Sci., *112:* 1835–1842, 1999.
4. Liotta, L. A., and Kohn, E. C. The microenvironment of the tumour-host interface. Nature (Lond.), *411:* 375–379, 2001.
5. Perou, C. M., Sorlie, T., Eisen, M. B., van de Rijn, M., Jeffrey, S. S., Rees, C. A., Pollack, J. R., Ross, D. T., Johnsen, H., Akslen, L. A., Fluge, O., Pergamenschikov, A., Williams, C., Zhu, S. X., Lonning, P. E., Borresen-Dale, A. L., Brown, P. O., and Botstein, D. Molecular portraits of human breast tumours. Nature (Lond.), *406:* 747–752, 2000.
6. Bonner, R. F., Emmert-Buck, M., Cole, K., Pohida, T., Chuaqui, R., Goldstein, S., and Liotta, L. A. Laser capture microdissection: molecular analysis of tissue. Science (Wash. DC), *278:* 1481, 1483, 1997.
7. Farina, K. L., Wyckoff, J. B., Rivera, J., Lee, H., Segall, J. E., Condeelis, J. S., and Jones, J. G. Cell motility of tumor cells visualized in living intact primary tumors using green fluorescent protein. Cancer Res., *58:* 2528–2532, 1998.
8. Wyckoff, J. B., Jones, J. G., Condeelis, J. S., and Segall, J. E. A critical step in metastasis: *in vivo* analysis of intravasation at the primary tumor. Cancer Res., *60:* 2504–2511, 2000.

9. Wyckoff, J. B., Insel, L., Khazaie, K., Lichtner, R. B., Condeelis, J. S., and Segall, J. E. Suppression of ruffling by the EGF receptor in chemotactic cells. Exp. Cell Res., *242:* 100–109, 1998.
10. Neri, A., Welch, D., Kawaguchi, T., and Nicolson, G. L. Development and biologic properties of malignant cell sublines and clones of a spontaneously metastasizing rat mammary adenocarcinoma. J. Natl. Cancer Inst. (Bethesda), *68:* 507–517, 1982.
11. Edmonds, B. T., Bell, A., Wyckoff, J., Condeelis, J., and Leyh, T. S. The effect of F-actin on the binding and hydrolysis of guanine nucleotide by *Dictyostelium* elongation factor 1A. J. Biol. Chem., *273:* 10288–10295, 1998.
12. Shestakova, E. A., Wyckoff, J., Jones, J., Singer, R. H., and Condeelis, J. Correlation of β-actin messenger RNA localization with metastatic potential in rat adenocarcinoma cell lines. Cancer Res., *59:* 1202–1205, 1999.
13. Centonze, V. E., and White, J. G. Multiphoton excitation provides optical sections from deeper within scattering specimens than confocal imaging. Biophys. J., *75:* 2015–2024, 1998.
14. Williams, R. M., Zipfel, W. R., and Webb, W. W. Multiphoton microscopy in biological research. Curr. Opin. Chem. Biol., *5:* 603–608, 2001.
15. Soll, D. R. The use of computers in understanding how animal cells crawl. Int. Rev. Cytol., *163:* 43–104, 1995.
16. Cheung, V. G., Morley, M., Aguilar, F., Massimi, A., Kucherlapati, R., and Childs, G. Making and reading microarrays. Nat. Genet., *21:* 15–19, 1999.
17. Zavadil, J., Bitzer, M., Liang, D., Yang, Y. C., Massimi, A., Kneitz, S., Piek, E., and Bottinger, E. P. Genetic programs of epithelial cell plasticity directed by transforming growth factor-β. Proc. Natl. Acad. Sci. USA, *98:* 6686–6691, 2001.
18. Chauhan, B. K., Reed, N. A., Zhang, W., Duncan, M. K., Kilimann, M. W., and Cvekl, A. Identification of genes downstream of Pax6 in the mouse lens using cDNA microarrays. J. Biol. Chem., *277:* 11539–11548, 2002.
19. Ross, A. F., Oleynikov, Y., Kislauskis, E. H., Taneja, K. L., and Singer, R. H. Characterization of a β-actin mRNA zipcode-binding protein. Mol. Cell. Biol., *17:* 2158–2165, 1997.
20. Edmonds, B. T., Wyckoff, J., Yeung, Y. G., Wang, Y., Stanley, E. R., Jones, J., Segall, J., and Condeelis, J. Elongation factor-1 α is an overexpressed actin binding protein in metastatic rat mammary adenocarcinoma. J. Cell Sci., *109:* 2705–2714, 1996.
21. Welch, M. D., DePace, A. H., Verma, S., Iwamatsu, A., and Mitchison, T. J. The human Arp2/3 complex is composed of evolutionarily conserved subunits and is localized to cellular regions of dynamic actin filament assembly. J. Cell Biol., *138:* 375–384, 1997.
22. Denk, W., Strickler, J. H., and Webb, W. W. Two-photon laser scanning fluorescence microscopy. Science (Wash. DC), *248:* 73–76, 1990.
23. Campagnola, P. J., Clark, H. A., Mohler, W. A., Lewis, A., and Loew, L. M. Second-harmonic imaging microscopy of living cells. J. Biomed. Opt., *6:* 277–286, 2001.
24. Bailly, M., Yan, L., Whitesides, G. M., Condeelis, J. S., and Segall, J. E. Regulation of protrusion shape and adhesion to the substratum during chemotactic responses of mammalian carcinoma cells. Exp. Cell Res., *241:* 285–299, 1998.
25. Wyckoff, J. B., Segall, J. E., and Condeelis, J. S. The collection of the motile population of cells from a living tumor. Cancer Res., *60:* 5401–5404, 2000.
26. Dong, G., Loukinova, E., Chen, Z., Gangi, L., Chanturita, T. I., Liu, E. T., and Van Waes, C. Molecular profiling of transformed and metastatic murine squamous carcinoma cells by differential display and cDNA microarray reveals altered expression of multiple genes related to growth, apoptosis, angiogenesis, and the NF-κB signal pathway. Cancer Res., *61:* 4797–4808, 2001.
27. Doyle, G. A., Betz, N. A., Leeds, P. F., Fleisig, A. J., Prokipcak, R. D., and Ross, J. The c-myc coding region determinant-binding protein: a member of a family of KH domain RNA-binding proteins. Nucleic Acids Res., *26:* 5036–5044, 1998.
28. Ross, J., Lemm, I., and Berberet, B. Overexpression of an mRNA-binding protein in human colorectal cancer. Oncogene, *20:* 6544–6550, 2001.
29. Zhang, J. Y., Chan, E. K., Peng, X. X., and Tan, E. M. A novel cytoplasmic protein with RNA-binding motifs is an autoantigen in human hepatocellular carcinoma. J. Exp. Med., *189:* 1101–1110, 1999.
30. Jesaitis, L. A., and Goodenough, D. A. Molecular characterization and tissue distribution of ZO-2, a tight junction protein homologous to ZO-1 and the *Drosophila* discs-large tumor suppressor protein. J. Cell Biol., *124:* 949–961, 1994.
31. Fitter, S., Sincock, P. M., Jolliffe, C. N., and Ashman, L. K. Transmembrane 4 superfamily protein CD151 (PETA-3) associates with β_1 and $\alpha_{IIb}\beta_3$ integrins in haemopoietic cell lines and modulates cell-cell adhesion. Biochem. J., *338:* 61–70, 1999.
32. Wei, P., Zhao, Y. G., Zhuang, L., Ruben, S., and Sang, Q. X. Expression and enzymatic activity of human disintegrin and metalloproteinase ADAM19/meltrin β. Biochem. Biophys. Res. Commun., *280:* 744–755, 2001.
33. Bailly, M., Ichetovkin, I., Grant, W., Zebda, N., Machesky, L. M., Segall, J. E., and Condeelis, J. The F-actin side binding activity of the Arp2/3 complex is essential for actin nucleation and lamellipod extension. Curr. Biol., *11:* 620–625, 2001.
34. Carlier, M. F. Control of actin dynamics. Curr. Opin. Cell Biol., *10:* 45–51, 1998.
35. Takaishi, K., Matozaki, T., Nakano, K., and Takai, Y. Multiple downstream signalling pathways from ROCK, a target molecule of Rho small G protein, in reorganization of the actin cytoskeleton in Madin-Darby canine kidney cells. Genes Cells, *5:* 929–936, 2000.
36. Weaver, A. M., Karginov, A. V., Kinley, A. W., Weed, S. A., Li, Y., Parsons, J. T., and Cooper, J. A. Cortactin promotes and stabilizes Arp2/3-induced actin filament network formation. Curr. Biol., *11:* 370–374, 2001.
37. Huang, P., and Oliff, A. Signaling pathways in apoptosis as potential targets for cancer therapy. Trends Cell Biol., *11:* 343–348, 2001.
38. Marion, R. M., Fortes, P., Beloso, A., Dotti, C., and Ortin, J. A human sequence homologue of Staufen is an RNA-binding protein that is associated with polysomes and localizes to the rough endoplasmic reticulum. Mol. Cell. Biol., 19*:* 2212–2219, 1999.
39. Liu, G., Grant, W. M., Persky, D., Latham, V. M., Jr., Singer, R. H., and Condeelis, J. Interactions of elongation factor 1α with F-actin and β-actin mRNA: implications for anchoring mRNA in cell protrusions. Mol. Biol. Cell, *13:* 579–592, 2002.
40. Kaufmann, A. M., Khazaie, K., Wiedemuth, M., Rohde-Schulz, B., Ullrich, A., Schirrmacher, V., and Lichtner, R. B. Expression of epidermal growth factor receptor correlates with metastatic potential of 13762NF rat mammary adenocarcinoma cells. Int. J. Oncol., *4:* 1149–1155, 1994.
41. Lanzetti, L., Rybin, V., Malabarba, M. G., Christoforidis, S., Scita, G., Zerial, M., and Di Fiore, P. P. The Eps8 protein coordinates EGF receptor signalling through Rac and trafficking through Rab5. Nature (Lond.), *408:* 374–377, 2000.
42. Zhang, W., Razani, B., Altschuler, Y., Bouzahzah, B., Mostov, K. E., Pestell, R. G., and Lisanti, M. P. Caveolin-1 inhibits epidermal growth factor-stimulated lamellipod extension and cell migration in metastatic mammary adenocarcinoma cells (MTLn3). Transformation suppressor effects of adenovirus-mediated gene delivery of caveolin-1. J. Biol. Chem., *275:* 20717–20725, 2000.
43. Sanders, L. C., Matsumura, F., Bokoch, G. M., and de Lanerolle, P. Inhibition of myosin light chain kinase by p21-activated kinase. Science (Wash. DC), *283:* 2083–2085, 1999.
44. Wozney, J. M., Rosen, V., Celeste, A. J., Mitsock, L. M., Whitters, M. J., Kriz, R. W., Hewick, R. M., and Wang, E. A. Novel regulators of bone formation: molecular clones and activities. Science (Wash. DC), *242:* 1528–1534, 1988.
45. Kessler, E., Takahara, K., Biniaminov, L., Brusel, M., and Greenspan, D. S. Bone morphogenetic protein-1: the type I procollagen C-proteinase. Science (Wash. DC), *271:* 360–362, 1996.
46. Sommers, C. L. The role of cadherin-mediated adhesion in breast cancer. J. Mammary Gland Biol. Neoplasia, *1:* 219–229, 1996.
47. Noe, V., Chastre, E., Bruyneel, E., Gespach, C., and Mareel, M. Extracellular regulation of cancer invasion: the E-cadherin-catenin and other pathways. Biochem. Soc. Symp., *65:* 43–62, 1999.
48. Ong, A., Maines-Bandiera, S. L., Roskelley, C. D., and Auersperg, N. An ovarian adenocarcinoma line derived from SV40/E-cadherin-transfected normal human ovarian surface epithelium. Int. J. Cancer, *85:* 430–437, 2000.
49. Calabro, A., Orsini, B., Renzi, D., Papi, L., Surrenti, E., Amorosi, A., Herbst, H., Milani, S., and Surrenti, C. Expression of epidermal growth factor, transforming growth factor-α and their receptor in the human oesophagus. Histochem. J., *29:* 745–758, 1997.
50. Peoples, G. E., Blotnick, S., Takahashi, K., Freeman, M. R., Klagsbrun, M., and Eberlein, T. J. T lymphocytes that infiltrate tumors and atherosclerotic plaques produce heparin-binding epidermal growth factor-like growth factor and basic fibroblast growth factor: a potential pathologic role. Proc. Natl. Acad. Sci. USA, *92:* 6547–6551, 1995.
51. Kume, N., and Gimbrone, M. A., Jr. Lysophosphatidylcholine transcriptionally induces growth factor gene expression in cultured human endothelial cells. J. Clin. Invest., *93:* 907–911, 1994.
52. Dluz, S. M., Higashiyama, S., Damm, D., Abraham, J. A., and Klagsbrun, M. Heparin-binding epidermal growth factor-like growth factor expression in cultured fetal human vascular smooth muscle cells. Induction of mRNA levels and secretion of active mitogen. J. Biol. Chem., *268:* 18330–18334, 1993.
53. Lichtner, R. B., Kaufmann, A. M., Kittmann, A., Rohde-Schulz, B., Walter, J., Williams, L., Ullrich, A., Schirrmacher, V., and Khazaie, K. Ligand mediated activation of ectopic EGF receptor promotes matrix protein adhesion and lung colonization of rat mammary adenocarcinoma cells. Oncogene, *10:* 1823–1832, 1995.
54. Kaufmann, A. M., Lichtner, R. B., Schirrmacher, V., and Khazaie, K. Induction of apoptosis by EGF receptor in rat mammary adenocarcinoma cells coincides with enhanced spontaneous tumour metastasis. Oncogene, *13:* 2349–2358, 1996.
55. Henderson, I. C., and Patek, A. J. The relationship between prognostic and predictive factors in the management of breast cancer. Breast Cancer Res. Treat., *52:* 261–288, 1998.
56. Shestakova, E. A., Singer, R. H., and Condeelis, J. The physiological significance of β-actin mRNA localization in determining cell polarity and directional motility. Proc. Natl. Acad. Sci. USA, *98:* 7045–7050, 2001.
57. Cooper, J. A., Wear, M. A., and Weaver, A. M. Arp2/3 complex: advances on the inner workings of a molecular machine. Cell, *107:* 703–705, 2001.
58. Maa, M. C., Wilson, L. K., Moyers, J. S., Vines, R. R., Parsons, J. T., and Parsons, S. J. Identification and characterization of a cytoskeleton-associated, epidermal growth factor sensitive pp60c-src substrate. Oncogene, *7:* 2429–2438, 1992.
59. Weed, S. A., and Parsons, J. T. Cortactin: coupling membrane dynamics to cortical actin assembly. Oncogene, *20:* 6418–6434, 2001.
60. Fournier, M. V., Carvalho, M. G., and Pardee, A. B. A strategy to identify genes associated with circulating solid tumor cell survival in peripheral blood. Mol. Med., *5:* 313–319, 1999.
61. Coulombe, P. A., and Omary, M. B. "Hard" and "soft" principles defining the structure, function and regulation of keratin intermediate filaments. Curr. Opin. Cell Biol., *14:* 110–122, 2002.